Direct electroreduction of oxides in molten fluoride salts

M. Gibilaro*, J. Pivato, L. Cassayre, L. Massot, P. Chamelot, P. Taxil

Laboratoire de Génie Chimique UPS/CNRS, Département Procédés Electrochimiques, Université de Toulouse, 118 route de Narbonne, 31062 Toulouse Cedex, France

Keywords:
Molten fluoride
Direct reduction
Metallic oxide
Pilling–Bedworth ratio

A B S T R A C T

A new kind of electrolyte composed of molten fluorides has been evaluated in order to perform a feasibility study of the direct electroreduction reaction. The direct reduction of SnO_2 and Fe_3O_4 was realised in LiF–NaF at 750 °C and in LiF–CaF_2 at 850 °C for TiO_2 and TiO. The electrochemical behaviour of these oxides was studied by linear sweep voltammetry: a current corresponding to the oxide reduction was evidenced for TiO_2, SnO_2 and Fe_3O_4. After galvanostatic electrolyses, a complete conversion was obtained for all oxides, except TiO, and the structure of reduced Ti and Fe samples had a typical coral-like structure while dense drops of Sn were recovered (Sn is liquid at operating temperature). After TiO electrolysis, a thin external metallic titanium layer was detected, acting as a barrier for the oxide ion diffusion and no complete reduction can be achieved. This could be explained by a Pilling–Bedworth ratio around 1 for Ti/TiO.

1. Introduction

In the last decade, a new electrochemical process has been developed in order to convert solid oxides into their metal: the direct electrochemical reduction. Chen et al. [1] have first achieved the direct reduction of TiO_2 into Ti in a molten chloride salt composed of $CaCl_2$. This innovative method is now often referred as the FFC (Fray–Farthing–Chen) Cambridge process, where the overall reaction is the oxygen removal from a solid M_xO_y oxide at the cathode (1) and the formation of $CO_2(g)$ at the carbon anode (2), according to:

$$M_xO_y(s) + 2ye^- = xM(s) + yO^{2-} \quad (1)$$

$$2O^{2-} + C(s) = CO_2(g) + 4e^- \quad (2)$$

The FFC process has been intensively studied worldwide, exclusively in molten chloride salts (LiCl or $CaCl_2$), for different purposes: high purity Si production [2], spent nuclear fuel processing (reduction of rare earth oxides [3], UO_2 [4], U_3O_8 [5], MOX [6], spent fuel [7], etc.), pure metal or alloy production (reduction of Nb_2O_5, Fe_2O_3, NiO–TiO_2, etc. [8–10]). No data are available in the literature for the electrochemical reduction of SnO_2, TiO and Fe_3O_4 whereas TiO_2 has been intensively studied in chloride salts [1,11–13]. In molten $CaCl_2$, its reduction pathway has been proposed [14] and several titanium sub-oxides have been characterised (Ti_4O_7, Ti_3O_5, Ti_2O_3, $CaTi_2O_4$).

However, up to now, no process has reached the industrial scal A recurrent problem is that the final product is often polluted b carbides, due to the reduction of carbonates CO_3^{2-} formed by th reaction of the $CO_2(g)$ anodic product with O^{2-} cations dissolve in the salt [15]. Furthermore, carbon particles coming from th anode often causes shortcuts in the cell. An option to avoid ca bide formation is to use an oxygen evolving anode, on which th electrochemical reaction is:

$$2O^{2-} = O_2(g) + 4e^- \quad (3$$

However, this reaction is difficult to control in chloride sal due to the close potentials of $Cl_2(g)$ and $O_2(g)$ evolution [4 and corrosion occurs on anodic materials like Pt [16] or SnC [17].

In this work, a different category of electrolyte was teste i.e. the molten fluorides, with the advantage of using an ine gold anode, allowing $O_2(g)$ evolution [18] as presented i Fig. 1(a). If the oxide concentration in these molten solven is high enough, corrosion of such anodic material will n occur.

The direct reduction was applied to four different oxides: SnC and Fe_3O_4 in LiF–NaF at $T = 750$ °C and TiO_2 and TiO in LiF–CaF at $T = 850$ °C, with the main purpose of the first assessment of th feasibility of the reduction reaction.

The first part of the work is dedicated to the electrochemic characterisation of oxide samples by linear sweep voltammetr Then, galvanostatic electrolyses have been performed on sma amounts of oxide pellets (~200–300 mg) and the reaction produc have been characterised by SEM-EDX and XRD.

* Corresponding author. Tel.: +33 561 558 677; fax: +33 561 556 139.
E-mail address: gibilaro@chimie.ups-tlse.fr (M. Gibilaro).

doi:10.1016/j.electacta.2011.02.109

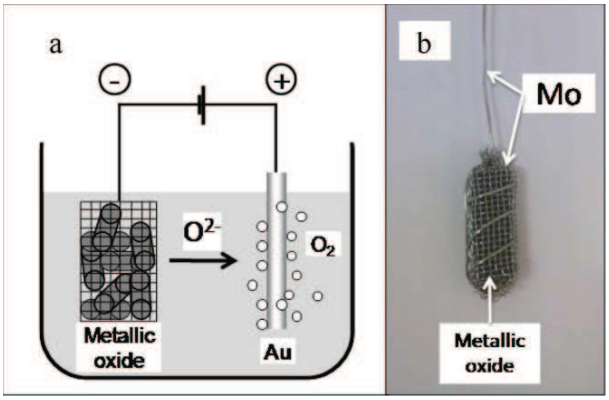

Fig. 1. (a) Schematic representation of the FFC Cambridge process and (b) picture of metallic oxide sample.

2. Experimental

The cell consisted of a vitreous carbon crucible placed in a cylindrical vessel made of refractory steel. The inner part of the walls was protected against fluoride vapours by a graphite liner. Experiments were performed under inert argon (U grade) atmosphere. More details can be found in a previous paper [19].

The electrolyte (200 g) was composed either of the eutectic LiF–CaF_2 (79–21 molar) or of the eutectic LiF–NaF (61–39 molar), from Carlo Erba Reagents (99.99%). The salt mixtures were dehydrated by heating under vacuum ($\sim 10^{-4}$ bar) from room temperature up to the melting point (767 °C and 649 °C respectively) for 72 h. 2 g of lithium oxide (Li_2O) powder (Cerac 99.5%) were added after salt melting to provide oxide ions into the bath. The Li_2O concentration was maintained at a concentration higher than 1 mass.% during electrochemical runs, ensuring that the anodic reaction corresponded to oxygen formation, and thus, preventing the gold oxidation.

TiO_2, TiO, SnO_2 and Fe_3O_4 were used in the form of sintered pellets (Alfa Aesar 99.9%). The oxide pellets, attached with a molybdenum grid connected to the current lead thanks to a molybdenum wire (Fig. 1(b)), were used as working electrodes. The auxiliary electrode was a gold wire with a large surface area ($S = 3.6\,cm^2$) and all potentials were referred to a platinum wire (0.5 mm diameter), acting as a quasi-reference electrode $Pt/PtO_x/O^{2-}$ [20].

The electrochemical experiments were performed with an Autolab PGSTAT 30 potentiostat/galvanostat. After resin embedding and polishing, the cathode bulk was examined with a scanning electron microscope (LEO 435 VP) equipped with an EDS probe (Oxford INCA 200). XRD characterisations were performed with a Diffractometer D5000 Siemens.

3. Results and discussion

3.1. Solvent selection

In order to perform the direct electrochemical reduction of a given metal oxide in fluoride mixtures, solvent selection is important: reduction of the metal oxide has to occur at a potential more positive than the alkaline/alkaline earth deposition one. A thermodynamical study has been carried out, using data from [21] and taking into consideration both the solvent components (metal, fluorides and oxides compounds) and the oxide to be reduced. The most common fluoride salts, composed of binary mixtures based on LiF, NaF, KF and CaF_2, have been taken into account.

Table 1
Standard free energy data related to the relative stability of Li, K, Na, Ca (Eq. (5)) and Li_2O, K_2O, Na_2O, CaO (Eq. (6)) in fluoride media (data from [21]).

Reaction	Standard free energy $\Delta_r G^\circ$ ($J\,mol^{-1}$) at 800 °C
KF(s) + Li(liq) = K(g) + LiF(s)	−52,892
NaF(s) + Li(liq) = Na(liq) + LiF(s)	−47,464
$0.5CaF_2$(s) + Li(liq) = 0.5Ca(s) + LiF(s)	13,137
K_2O(liq) + 2LiF(s) = 2KF(s) + Li_2O(s)	−139,381
Na_2O(s) + 2LiF(s) = 2NaF(s) + Li_2O(s)	−90,582
CaO(s) + 2LiF(s) = CaF_2(s) + Li_2O(s)	39,935

(i) The Gibbs energy ($\Delta_r G^\circ$) of the reaction between a metal oxide and an alkaline metal indicates whether the oxide is reduced by the alkaline:

$$M_xO_y + ymA = xM + yA_mO \quad (A = Li, Na, K, Ca; m = 1, 2) \tag{4}$$

If $\Delta_r G^\circ$ is negative, the oxide reduction occurs at a potential more positive than the solvent alkaline deposition and the direct reduction is then achievable thermodynamically. If $\Delta_r G^\circ$ is positive, an A_mO activity decrease (i.e. a decrease of its concentration in the molten salt) may allow the reduction reaction to occur [22].

(ii) Since binary fluoride mixtures are considered, the relative stability of alkaline/alkaline earth metal has to be established, in order to determine which A-compound is involved in Eq. (4):

$$1/nAF_n + B = 1/n\,A + BF \quad (A, B = Li, Na, K, Ca; n = 1, 2) \tag{5}$$

Calculated standard free energy data at 800 °C related to Eq. (5) are compiled in Table 1, considering the LiF/Li redox system as a reference (B = Li in Eq. (5)): the Gibbs energy of reaction (5) is negative for KF and NaF compounds, meaning that they are reduced at a more positive potential than LiF. On the other hand, CaF_2 is reduced at a potential more negative than LiF. The relative stability of the metals, which is valid in the 500–1000 °C temperature range, is thus: Ca < Li < Na < K. As a consequence, in the case of the reduction in LiF–CaF_2 mixtures, the first metal to be formed will be Li, while Na is favored in LiF–NaF mixtures.

(iii) A last equilibrium to consider in the case of the direct reduction of metal oxides in binary fluoride mixtures is the relative stability of the alkaline oxides produced according to Eq. (4). Indeed the oxide A_mO related to the most stable alkaline is likely to react with the fluoride compound $BF_{2/m}$ of the less stable alkaline according to:

$$A_mO + 2BF = mAF_{2/m} + B_2O \quad (A, B = Li, Na, K, Ca; m = 1, 2) \tag{6}$$

The Gibbs energy of reaction (6), indicated in Table 1 with LiF/Li_2O as a reference (B = Li in Eq. (6)), allows a relative stability of oxides to be established: CaO > Li_2O > Na_2O > K_2O.

(iv) Combining Eqs. (4) and (6), the overall general reaction to be considered in a binary system is:

$$M_xO_y + ymA + ypBF_{2/p} = xM + ymAF_{2/m} + yB_pO \quad (A, B = Ca, Li, Na, K; m, p = 1, 2) \tag{7}$$

As discussed for Eq. (4), if $\Delta_r G^\circ$ of reaction (7) is negative, the metal oxide reduction should occur at a potential more pos-

Table 2
Standard free energy of various reduction reactions based on Eq. (7); maximum Li_2O/CaO activity for the reduction of metal oxides at 750 °C/850 °C (data from [21]); $a(AF_n)$ is the activity of the solvent components.

LiF–NaF eutectic at 750 °C	Standard free energy of reaction $\Delta_r G^\circ$ (J mol^{-1})	Maximum Li_2O activity
a(LiF) = 0.6; a(NaF) = 0.4		
$Fe_3O_4(s) + 8Na(liq) + 8LiF(s) = 3Fe(s) + 8NaF(s) + 4Li_2O(s)$	−720,164	1
$SnO_{2(s)} + 4Na(liq) + 4LiF(s) = Sn(liq) + 4NaF(s) + 2Li_2O(s)$	−398,486	1
$TiO_2(s) + 4Na(liq) + 4LiF(s) = Ti(s) + 4NaF(s) + 2Li_2O(s)$	6662	0.68
$TiO(s) + 2Na(liq) + 2LiF(s) = Ti(s) + 2NaF(s) + Li_2O(s)$	68,084	3.3×10^{-4}
LiF–CaF_2 eutectic at 850 °C	**Standard free energy of reaction $\Delta_r G^\circ$ (J mol^{-1})**	**Maximum CaO activity**
a(LiF) = 0.8; a(CaF_2) = 0.2		
$Fe_3O_4(s) + 8Li(liq) + 4CaF_2(s) = 3Fe(s) + 8LiF(s) + 4CaO(s)$	−1,161,343	1
$SnO_2(s) + 4Li(liq) + 2CaF_2(s) = Sn(liq) + 4LiF(s) + 2CaO(s)$	−615,693	1
$TiO_2(s) + 4Li(liq) + 2CaF_2(s) = Ti(s) + 4LiF(s) + 2CaO(s)$	−216,432	1
$TiO(s) + 2Li(liq) + CaF_2(s) = Ti(s) + 2LiF(s) + CaO(s)$	−43,810	1

itive than the formation of the most stable alkaline. Table 2 shows the calculated maximum A_mO activity (pure solid A_mO as reference state) below which reduction is favored according to Eq. (7). Only two common eutectic systems were considered in the first approach: LiF–CaF_2 (61–39 molar) at 850 °C, for which A = Li and B = Ca in Eq. (7), and LiF–NaF (79–21 molar) at 750 °C, with A = Na and B = Li. The activity of the fluoride compounds was considered equal to their molar fraction for the Gibbs energy calculations.

It comes from Table 2 that all considered oxides can be reduced in the LiF–CaF_2 eutectic at any Li_2O concentration while, in the LiF–NaF eutectic, Na_2O activity has to be lower than 0.0003 and 0.68 for TiO and TiO_2 compounds respectively. LiF–NaF solvent was thus not considered to be adapted to the reduction of titanium metal oxides, since such salt mixtures would require a careful control of the oxide concentration.

According to these thermochemical considerations, the direct electroreduction of SnO_2 and Fe_3O_4 has been investigated in the eutectic LiF–NaF at 750 °C while the eutectic LiF–CaF_2 at a working temperature of 850 °C was selected for titanium oxides.

3.2. Electrochemical study

The electrochemical behaviour of the four oxides was studied by linear sweep voltammetry at low scan rate (5 mV s^{-1}). Potentials were referred to the solvent reduction, either Li^+/Li for LiF–CaF_2 or Na^+/Na for LiF-NaF, and are reported as follows: V vs. X (X = Li or Na).

A linear voltammogram for TiO_2 in LiF–CaF_2–Li_2O at 850 °C is presented in Fig. 2. From 0 to 0.45 V vs. Li, an additional cathodic current is measured and attributed to the direct reduction of titanium dioxide. The same electrochemical technique was applied for TiO characterisation, but no signal corresponding to the reduction of TiO was evidenced. This was attributed to the low electronic conductivity of TiO, which, unlike TiO_2, does not form conductive Magnelli phases TiO_{2-x} at the early stage of the direct reduction process [23].

The SnO_2 and Fe_3O_4 electrochemical characterisation is represented in Fig. 3. Significant reduction currents are observed respectively at 1.3 and 0.6 V vs. Na and are attributed to the direct reduction reaction. Moreover, these oxides are easier to reduce than titanium oxides compounds, since their reduction potential is much more anodic than the solvent reduction potential.

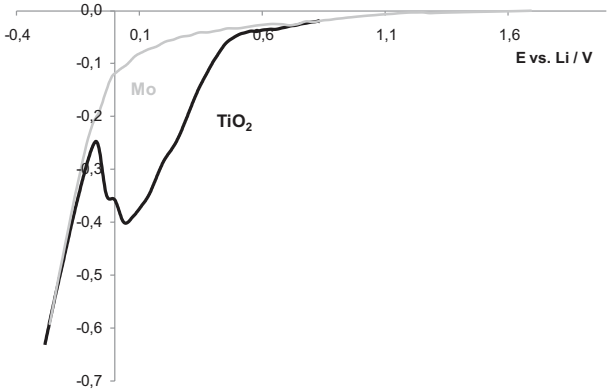

Fig. 2. Linear sweep voltammograms on Mo ($S = 0.31$ cm^2) and TiO_2 at 5 mV s^{-1} in LiF–CaF_2–Li_2O (1 mass.%) at $T = 850$ °C.

3.3. Product characterisation after direct reduction runs

Direct reduction experiments have been conducted in constant-current mode, for different intensities and durations.

Fig. 4 presents a superimposition of one of the electrolyses realised in LiF–NaF at 750 °C on Fe_3O_4 and SnO_2. The measured potential is very stable and always higher than the reduction potential of the solvent cation, meaning that the major part of the current has been used for the metal oxide direct reduction.

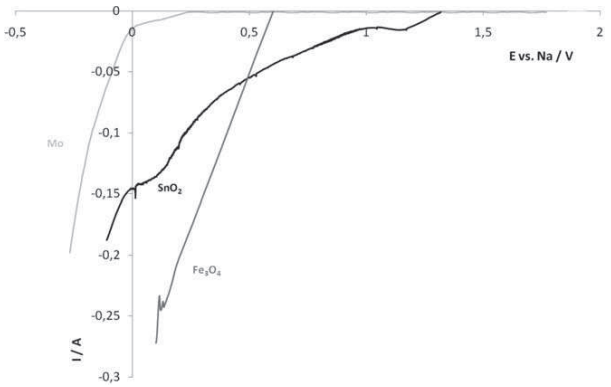

Fig. 3. Linear sweep voltammograms on Mo ($S = 0.31$ cm^2), SnO_2 and Fe_3O_4 at 5 mV s^{-1} in LiF–NaF–Li_2O (1 mass.%) at $T = 750$ °C.

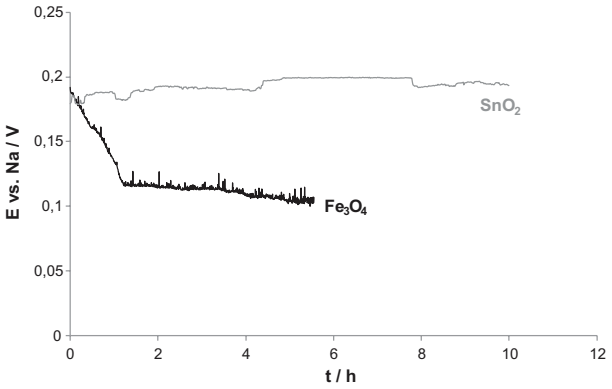

Fig. 4. SnO_2 and F_3O_4 electrode potentials during galvanostatic electrolysis versus time at 750 °C in LiF–NaF–Li_2O (1 mass.%).

The cross section of Fe_3O_4 pellets after direct electroreduction realised in different experimental conditions are presented in Fig. 5. In Fig. 5(a), for $I = -0.04$ A, $t = 20{,}000$ s and $m = 284$ mg, the SEM-EDX analysis indicates the presence of FeO, metallic Fe and no more Fe_3O_4. From the partially reduced sample, the following reduction pathway is proposed:

$$Fe_3O_4 + 2e^- = 3FeO + O^{2-} \quad (8)$$

$$FeO + 2e^- = Fe + O^{2-} \quad (9)$$

The inner layer of the metallic grain is composed of FeO whereas the external layer is formed of metallic Fe: the direct reduction of Fe_3O_4 took place progressively from the outside of the pellet.

A complete conversion of Fe_3O_4 pellet into metallic iron, presented in Fig. 5(b), has been obtained when a higher electrical charge imposed: $I = -0.1$ A, $t = 10{,}000$ s and $m = 275$ mg. No oxide phase was detected and the sample was only composed of Fe and frozen salts. The resulting product was very porous and had a coral-like structure due to the oxygen removal. This typical pattern is commonly obtained after the direct reduction of oxides, as UO_2 in molten chlorides [24].

The reduction pathway observed on SnO_2 in LiF–NaF at 750 °C is:

$$SnO_2(s) + 2e^- = SnO(s) + O^{2-} \quad (10)$$

$$SnO(s) + 2e^- = Sn(liq) + O^{2-} \quad (11)$$

The presence of SnO, illustrated in Fig. 6(a), was detected on the partially reduced sample ($m = 210$ g) close to the electrode surface and some Sn, which is liquid at the operating temperature, was found adhering on the Mo basket. The major part of metallic Sn had sunk at the bottom of the crucible and coalesced to form small balls recovered after the experiment cooling, as pictured in Fig. 6(b). The current efficiency, determined from the mass of recovered Sn, was found to be around 75%.

For TiO_2 ($m = 298$ mg), a complete reduction was achieved in LiF–CaF_2 at $I = -0.1$ A and $t = 60{,}000$ s. The cross section is presented in Fig. 7. Similarly to the Fe system, the characteristic sponge-like structure was observed with a homogeneous reduced material. In the partly converted sample, XRD analyses indicated the presence of salt components (Li_2O, CaO, LiF, CaF_2), metallic titanium and a $LiTiO_2$ compound. Moreover, in these analyses, no carbide phases were detected which supports the use of a gold anode for fluoride molten salts experiments.

Due to the sponge-like structure, some frozen salt is inserted into the final metallic product. Several methods are available for metal/salt separation: the van Arkel process [25], the arc melting method [26] or the distillation under vacuum [27]. The pyro-vacuum distillation could be envisaged and has been recently applied by Kapoor et al. [28] for the purification of zirconium produced in chloride salts. This process could be applied to the fluoride salts, but the purification step has not been studied in this work.

The current efficiency is quite low, around 25%, for the fully reduced TiO_2 sample. In Fig. 8, the electrolysis potential versus time is presented, where, at the beginning of the electrolysis, the electrode potential is lower than the solvent reduction. Some of the current was then used for the solvent deposition leading to a low current efficiency. To increase the current efficiency, the current should be stepwise decreased during the experiment to avoid the solvent ion reduction.

As no electrochemical signals were obtained for TiO, the electrolysis was performed in the same conditions as for TiO_2: $I = -0.1$ A and $t = 60{,}000$ s. The external part of the TiO sample observed by SEM (Fig. 9) was converted into pure Ti metal (thickness around 10 μm); but the bulk of the pellet still remained as TiO starting material. A possible explanation could be provided by Pilling–Bedworth rule [29] considerations: as proposed by Li et al. [30] in the case of oxide layer reduction, if the molar volume of the formed metal V_m is smaller than the molar volume of the oxide V_o, the formed metal on the oxide surface is porous enough to allow the molten salt electrolyte accessing to the underlying oxide. Thus the respect of this condition is required to successfully perform the

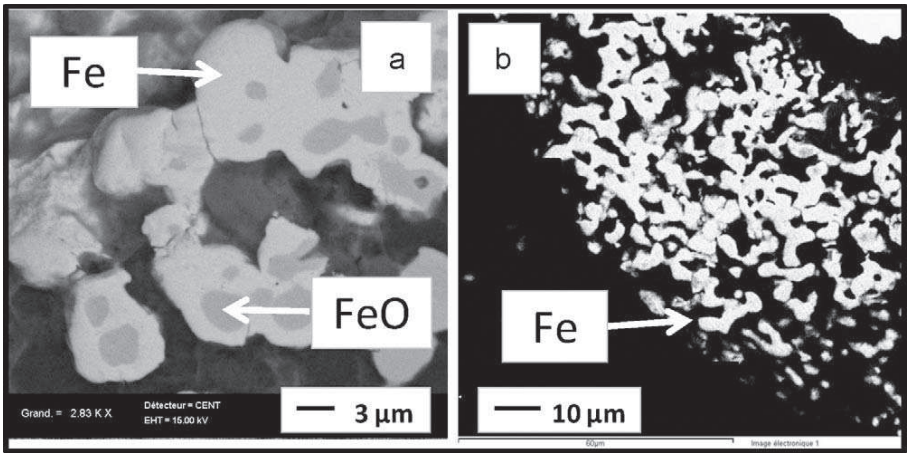

Fig. 5. Micrographs cross section of Fe_3O_4 sample after electrolysis. Experimental conditions: LiF–NaF–Li_2O (1 mass.%), $T = 750$ °C; (a) $I = -0.04$ A, $t = 20{,}000$ s; (b) $I = -0.1$ A, $t = 10{,}000$ s.

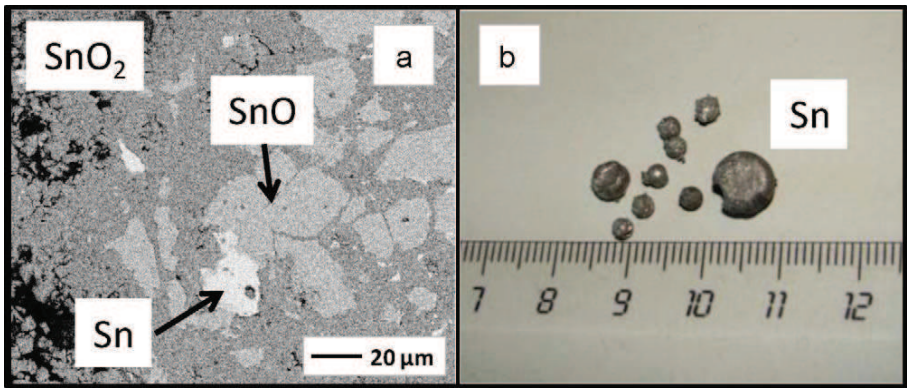

Fig. 6. (a) Micrograph cross section of SnO_2 after electrolysis in LiF–NaF–Li_2O (1 mass.%) and (b) picture of Sn balls found in the bottom of the crucible.

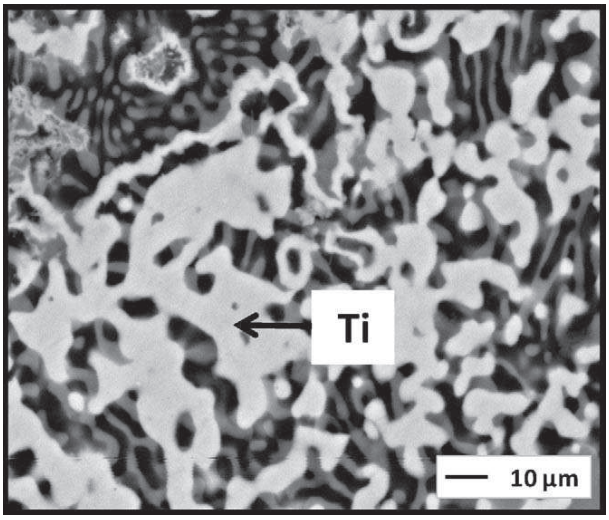

Fig. 7. Micrograph cross section of TiO_2 after electrolysis in LiF–CaF_2–Li_2O (1 mass.%), $T = 850\,^{\circ}C$, $I = -0.1$ A, $t = 60{,}000$ s.

direct electrochemical reduction within the bulk of the oxide:

$$\frac{V_m}{V_o} < 1 \quad \text{with} \quad V_m = \frac{M_m}{\rho_m} \text{ and } V_o = \frac{M_o}{\rho_o}$$

where M is the molar mass, ρ is the density and n the number of metal atoms in the oxide formula.

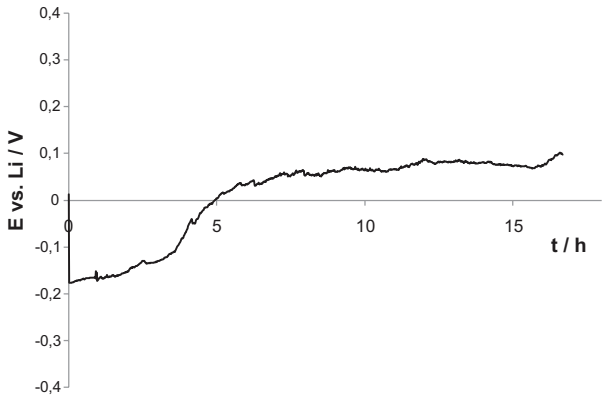

Fig. 8. TiO_2 electrode potential during galvanostatic electrolysis versus time at 850 °C in LiF–CaF_2–Li_2O (1 mass.%), $T = 850\,^{\circ}C$, $I = -0.1$ A, $t = 60{,}000$ s.

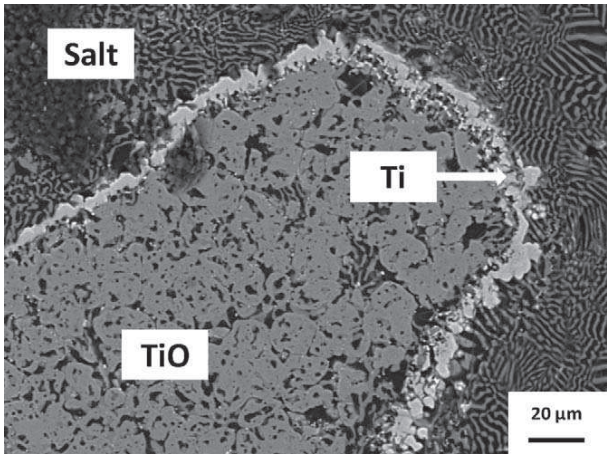

Fig. 9. Micrograph cross section of TiO after electrolysis in LiF–CaF_2–Li_2O (1 mass.%), $T = 850\,^{\circ}C$, $I = -0.1$ A, $t = 60{,}000$ s.

Table 3
Metal to oxide molar volume ratios.

M/M_{ox}	Fe/Fe_3O_4	Ti/TiO_2	Ti/TiO
V_m/V_o	0.47	0.56	0.86

In Table 3 are gathered the metal to oxide molar volume ratios for the different metal oxides studied in this paper. The SnO_2/Sn system was not considered since the formation of liquid Sn implies a constantly renewed oxide surface. Except for TiO, the calculated ratios are around 0.5, meaning that a noticeable volume constriction occurs during oxide conversion into metal. This observation is in agreement with our experiments concerning TiO_2 and Fe_3O_4: a complete conversion is achievable, and a porous metal phase is produced. But for TiO, the metal to oxide molar volume ratio is close to 1: the molar volumes are then approximately equal. The reduction is thus kinetically difficult because the diffusion of the generated oxide ions towards the electrolyte is hindered by the formation of a dense metal layer: the metal surface covers the whole oxide layer and forms a barrier to the solid state electroreduction, as observed in Fig. 9.

4. Conclusions

In replacement of the usual chloride molten salts ($CaCl_2$ and LiCl), fluoride salt mixtures have been used for the first time in this work in order to evaluate their potentialities as electrolytes for the

direct electrochemical reduction of oxide phases (TiO, TiO_2, SnO_2 and Fe_3O_4). An inert oxygen-evolving gold electrode was used as anode, instead of the commonly carbon one which produces CO_2 and leads to the formation of carbides in the reduced cathodic product. The gold anode was not attacked, as virtually no weight loss was observed; the same gold spiral has been reused in all experiments. Tests at larger scale may allow some anode corrosion to be evidenced, but this was not the purpose of the present paper, which was more focused on the feasibility study of the reduction reactions.

TiO was slightly reduced with an external Ti layer of 10 μm. This layer blocked the oxide ion diffusion to the anode and thus, stopped the reaction progress; as proposed by Li et al. [30], the ratio of molar volumes of metal and oxide appears to be a very important parameter which strongly affects the oxide to metal conversion. In all the electroreduced samples, XRD analysis did not reveal the presence of any carbide phase. For three of them (TiO_2, SnO_2 and Fe_3O_4), a complete conversion to metal was achieved.

Acknowledgments

This work was supported by the European ACSEPT (FP7-CP-2007-211 267) program.

References

[1] G.Z. Chen, D.J. Fray, T.W. Farthing, Nature 407 (2000) 361.
[2] K. Yasuda, T. Nohira, R. Hagiwara, Y.H. Ogata, Electrochim. Acta 53 (2007) 106.
[3] K. Hirota, T.H. Okabe, F. Saito, Y. Waseda, K.T. Jacob, J. Alloy Compd. 282 (1999) 101.
[4] Y. Sakamura, M. Kurata, T. Inoue, J. Electrochem. Soc. 153 (3) (2006) D31.
[5] S.M. Jeong, S.B. Park, S.S. Hong, C.S. Seo, S.W. Park, J. Radioanal. Nucl. Chem. 268 (2) (2006) 349.
[6] M. Iizuka, T. Inoue, M. Ougier, J.-P. Glatz, J. Nucl. Sci. Technol. 44 (5) (2007) 801.
[7] S.D. Herrmann, S.X. Li, Nucl. Technol. 171 (3) (2010) 247.
[8] S.M. Jeong, J.Y. Jung, C.S. Seo, S.W. Park, J. Alloy Compd. 440 (2007) 210.
[9] S.I. Wang, G.M. Haarberg, E. Kvalheim, J. Iron Steel Res. 16 (2008) 48.
[10] Y. Zhu, M. Ma, D. Wang, K. Jiang, X. Hu, X. Jin, G.Z. Chen, Chin. Sci. Bull. 51 (20) (2006) 2535.
[11] G.Z. Chen, D.J. Fray, J. Electrochem. Soc. 149 (2002) E455.
[12] D.T.L. Alexander, C. Schwandt, D.J. Fray, Acta Mater. 54 (2006) 2933.
[13] M. Liu, Z. Guo, W. Lu, Trans. Inst. Min. Metall. C 114 (2005) C87.
[14] C. Schwandt, D.J. Fray, Electrochim. Acta 51 (2005) 66.
[15] V.A. Lebedev, V.I. Sal'nikov, I.A. Sizikov, D.A. Rymkevich, Russ. J. Appl. Chem. 80 (9) (2007) 1503.
[16] S.M. Jeong, H.S. Shin, S.H. Cho, J.M. Hur, H.S. Lee, Electrochim. Acta 54 (2009) 6335.
[17] K.T. Kilby, S. Jiao, D.J. Fray, Electrochim. Acta 55 (2010) 7126.
[18] L. Massot, L. Cassayre, P. Chamelot, P. Taxil, J. Electroanal. Chem. 606 (2007) 17.
[19] P. Chamelot, P. Taxil, B. Lafage, Electrochim. Acta 39 (1994) 2571.
[20] A.D. Graves, D. Inman, Nature 208 (1965) 481.
[21] I. Barin, O. Knacke, O. Kubaschewski, Thermochemical Properties of Inorganic Substances, Springer-Verlag, Berlin, 1977.
[22] K. Gourishankar, L. Redey, M. Williamson, Light Metals (2002) 1075.
[23] H. Grauber, E. Krautz, Phys. Stat. Sol. A 69 (1982) 287.
[24] M. Iizuka, Y. Sakamura, T. Inoue, J. Nucl. Mater. 359 (2006) 102.
[25] A.E. van Arkel, J.H. de Boer, Z. Anorg. Allg. 148 (1) (1925) 345–350.
[26] G.L. Miller, Vacuum 4 (1954) 168–175.
[27] R.A. Beall, Bureau of Mines 646 (1968) 151.
[28] K. Kapoor, C. Padmaprabu, D. Nandi, Mater. Charac. 59 (2008) 213–222.
[29] N.B. Pilling, R.E. Bedworth, J. Inst. Met. 29 (1923) 529.
[30] W. Li, X. Jin, F. Huang, G.Z. Chen, Angew. Chem. Int. Ed. 49 (2010) 3203.